ELSEVIER

Bone 38 (2006) 878–887

BONE

www.elsevier.com/locate/bone

Re-evaluating the toughness of human cortical bone

Q.D. Yang [a,*], B.N. Cox [a], R.K. Nalla [b], R.O. Ritchie [b]

[a] *Rockwell Scientific Co. LLC, 1049 Camino Dos Rios, Thousand Oaks, CA 91360, USA*
[b] *Materials Sciences Division, Lawrence Berkeley National Laboratory, and University of California, Berkeley, CA 94720, USA*

Received 14 February 2005; revised 18 October 2005; accepted 26 October 2005
Available online 9 December 2006

Abstract

Data for fracture in human humeral cortical bone are re-analyzed to assess the validity for this material of linear-elastic fracture mechanics (LEFM), which is the standard method of analyzing toughness and one basis for analyzing clinical data relating to bone quality. A nonlinear fracture model, which is based on representing the damage zone in the bone by a cohesive model, is calibrated against a number of sets of test data for normal (not diseased or aged) human cortical bone taken from cadavers. The data consist of load vs. load-point displacement measurements from standard compact–tension fracture tests. Conventional LEFM is unable to account for the shape of the load–displacement curves, but the nonlinear model overcomes this deficiency. Calibration of the nonlinear model against one data curve leads to predictions of the peak load and the displacement to peak load for two other data curves that are, for this limited test set, more accurate than those made using LEFM. Furthermore, prior observations of damage mechanisms in bone are incompatible with the modeling assumption of LEFM that all nonlinearity is confined to a zone much smaller than the specimen and the crack length. The predictions of the cohesive model and the prior observations concur that the length of the nonlinear zone in human cortical bone varies in the range 3–10 mm, which is comparable to or larger than naturally-occurring bones and the specimens used to test them. We infer that LEFM is not an accurate model for cortical bone. The fracture toughness of bone deduced via LEFM from test data will not generally be a material constant, but will take different values for different crack lengths and test configurations. The accuracy of using LEFM or single-parameter fracture toughness for analyzing the significance of data from clinical studies is called into question. The nonlinear cohesive zone model is proposed to be a more accurate model of bone and the traction-displacement or cohesive law is hypothesized to be a material property. The cohesive law contains a more complete representation of the mechanics of material failure than the single-parameter fracture toughness and may therefore provide a superior measure of bone quality, e.g., for assessing the efficacy of therapy for osteoporosis.

Keywords: Cortical bone; Fracture; Toughness; Cohesive zone

Introduction

Cortical bone is a natural composite with an organic component, mainly collagen, and a mineral apatite phase, arranged in a complex, hierarchical structure [41]. Akin to engineering composite materials, experiments show that damage initiates as diffuse but discrete strain localization events distributed in space in a way that is strongly correlated with the heterogeneous structure. The localizations include damage bands that continue to transfer stress into the surrounding material and microcracks, which are traction-free. Under some conditions, such distributed damage evolves into a single dominant crack, around the tip of which the diffuse damage events continue to occur as part of the crack-growth process. To date, most assessments of the toughness of bone, which represents a macroscopic characterization of such processes, have involved linear-elastic fracture mechanics (LEFM) analyses, which yield a single-valued fracture toughness, K_{Ic}. This has proved to be an important concept as it is one measure of the probability of fracture and hence of bone quality. Thus, toughness evaluated using LEFM is one possible basis for analyzing the effect of drug therapies on bone quality, using fracture data from either animal models or cadavers. However, due to the size-scales involved, LEFM may not represent an accurate or physically correct approach. In this work, we show that the complexity of fracture in cortical bone, over dimensions comparable to those in the human skeleton, warrants a more detailed (nonlinear) evaluation of such fracture instability. In light of this, we believe that nonlinear methods

* Corresponding author.
E-mail address: qyang@rwsc.com (Q.D. Yang).

8756-3282/$ - see front matter © 2005 Elsevier Inc. All rights reserved.
doi:10.1016/j.bone.2005.10.014

ought to be considered for analyzing either animal models or clinical data.

Background

Linear fracture models of bone

Prior mechanical descriptions of fracture in cortical bone, based on LEFM, assume that the toughness is a material constant identified with a point process at the crack tip. Any inelastic behavior is assumed to be limited to a small near-tip region (small-scale yielding) so that the stress and displacement fields local to the tip of a pre-existing crack can be described, for mode I loading, by the stress–intensity factor, K_I. The resistance to fracture, or fracture toughness, is then defined for a particular loading mode as the critical stress–intensity value, K_{Ic}, at the onset of unstable fracture.[1] This critical value has been assumed to be a material constant for a particular specimen, although it has been recognized to vary with age, disease, environmental exposure, and the location and orientation of the bone specimen, among other factors [7–9,32,38,39,54,57,58]. When regarded as an undamaged continuum, bone has also been recognized to have anisotropic and rate-dependent properties. Microstructural anisotropy accounts for a marked anisotropy observed in fracture resistance, e.g., between cracks growing parallel and normal to the axis of the osteon structures. Specifically, cortical bone is much tougher (typically by a factor of two) in the transverse orientation, where the crack must cut the osteons, in part due to the fact that the crack tends to deflect along the cement lines [8,35]. The toughness has also been described as rate-dependent, corresponding to subcritical crack growth, which can occur under both sustained and cyclic (fatigue) loading [33,35], and to be variable with respect to such factors as size and type of bone, anatomical location, material history, thickness, organic content, mineral distribution, degree of hydration, and age (for a recent review, see [44]).

Recently, a new series of papers have challenged the LEFM paradigm for fracture in cortical bone. Most notably, it has been recognized that the fracture toughness cannot be characterized by a single-value toughness, and that cracking behavior must be described in terms of a so-called crack-resistance curve (or *R*-curve), where the driving force for cracking increases with crack extension [30,35,51–53]. Implicit in this behavior are the origins of the toughness of bone, which are now believed primarily to involve mechanisms such as crack bridging that operate in the crack wake [43].

A key observation that is most germane to this viewpoint is that high-resolution imaging of cracks in human cortical bone shows that the crack advances as a complex system of mother–daughter cracks; microcracks are spawned ahead of and around the primary crack and link back to it only after lands of intact material deform and break after further loading (Fig. 1) [32,35,36]. The zone of microcracks and intact lands can be depicted as a bridging zone at the leading edge of the dominant crack, in a single crack idealization. The bridging is provided by uncracked ligaments,[2] which continue to transfer some stress across the zone of damaged material, thus shielding the crack tip from the applied load. The size of the bridges can range from a few to hundreds of micrometers. Their pattern is strongly correlated with the heterogeneity of the bone, e.g., microcracks appear to be associated with the osteon structures [35]. The total length, λ_b, of the zone of such bridges in the crack wake is a primary characteristic of the fracture process; in human cortical bone, this bridging zone can be quite large, i.e., $\lambda_b \sim 5$ mm [27,28,35,36].[3]

The very fact that observed bridging zones (or nonlinear process zones) are so large and thus of the same order of magnitude as the thickness of the cortical layer, at once calls into question the validity of LEFM. When a fracture process zone is commensurate with the structure, a condition known as large-scale bridging or yielding [16], the fracture toughness is no longer a material constant [3,5,11,12,16,18,26,29,42,45,46,50]. For a single (mother) crack with a process zone, the toughness K_{Ic} depends on extrinsic factors such as the specimen shape and loading configuration, because the contribution to toughening arising from bridging, K_b, is not independent of crack length (e.g., [5,13,14]). In such systems, the fracture properties can only be correctly accounted for by determining the constitutive behavior of the bridging process.

Methods

Nonlinear models for bone

In this paper, nonlinear fracture formulations will be shown to account for important features in fracture data for human cortical bone. The formulations are based on those developed for structural materials, where they have proven accurate and practicable [47]. Attention will be restricted to the problem of a single dominant crack, around which numerous microcracks or other nonlinear material events will usually occur, within a nonlinear fracture process zone, as shown schematically in Fig. 1a. Tests in which a single dominant crack is induced, e.g., from a sharp, machined notch, are a standard method for assessing the fracture resistance of bone. We believe that the analysis of nonlinear aspects of dominant-crack fracture will constitute one element of a strategy of formulating high-fidelity models of bone, in which diffuse, discrete damage events are modeled in sufficient detail at different scales to predict the relation of bone morphology and composition to macroscopic properties. Such high-fidelity models have potential clinical importance in identifying factors that control bone quality and determining whether they are amenable to therapy.

The nonlinear fracture model used for this analysis is the line-spring idealization [6,21,45,49], in which changes in the displacement fields around a crack that are due to a diffuse fracture process zone are collapsed into a

[1] The fracture toughness, K_{Ic}, may be defined as the critical value of the stress intensity K_I at the onset of unstable fracture at a pre-existing crack under mode I (tensile opening) conditions, i.e., when $K_I = Y\sigma_{app}(\pi a)^{1/2} = K_{Ic}$, where σ_{app} is the applied stress, a is the crack length, and Y is a function (of order unity) of crack size and geometry. Alternatively, the toughness can be expressed as a critical value of the strain–energy release rate, G_{Ic}, defined as the change in potential energy per unit increase in crack area. For an isotropic material loaded in mode I, $G_{Ic} = K_{Ic}^2/E'$, where $E' = E$ in plane stress and $E' = E/(1 - \nu^2)$ in plane strain (E is Young's modulus, ν is Poisson's ratio).

[2] In the context of fracture, "ligament" here refers to any unfailed material i.e., a crack "bridge", of any type, shape, and size, that spans the crack; not a ligament in the anatomical sense.

[3] Other mechanisms of crack bridging, for example intact collagen fibers that span the crack, have been identified in bone [22,59]. Collagen fibers can generate significant tractions at small crack displacements and therefore can be an especially significant contribution to toughening for cracks at the micron scale [37].

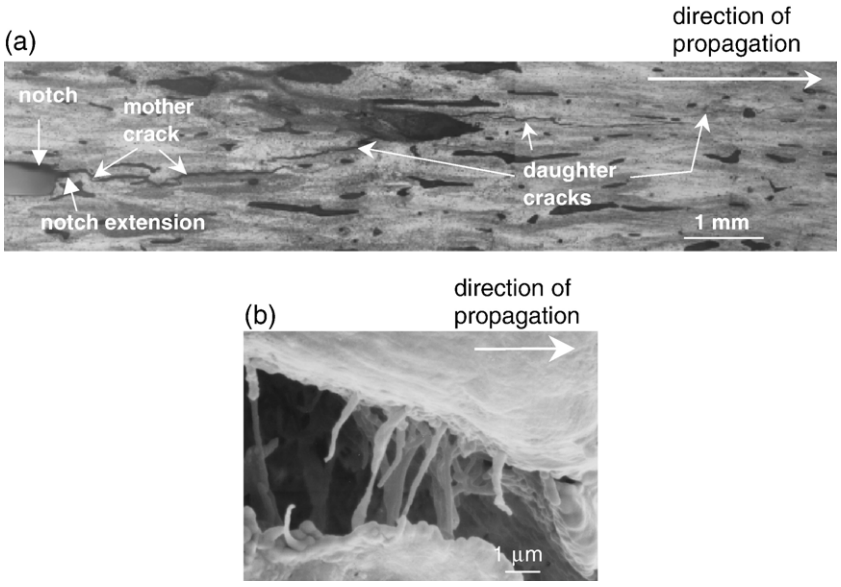

Fig. 1. (a) An optical micrograph of a crack in 61-year-old human cortical bone. Note the formation of daughter cracks and corresponding uncracked ligaments [36]. (b) Bridging by collagen fibrils in the wake of a crack in human cortical bone [36].

displacement discontinuity existing across a surface. Since the displacement jump accounts for material nonlinearity, the idealization allows the rest of the body to be treated as linear material (Fig. 2b). In mode I, the displacement discontinuity, $2u$, is defined to equal the net nonlinearity across the whole zone in the real material. For a plane problem in which the crack propagates in the x_1 direction along $x_3 = 0$:

$$u(x_1) = \int_0^{w_b(x_1)} \varepsilon_{33}^{p}(x_1, x_3)\, dx_3, \tag{1}$$

where $2w_b(x_1)$ is the width of the nonlinear damage zone at position x_1, and $\varepsilon_{ij}^{(p)}$ is the plastic strain tensor, i.e., the excess strain above that expected for linear, undamaged material under the same local stress state. The plastic strain need not, and generally will not, be uniform in the damage zone; it may incorporate localization events, including microcracks.

A traction field, p, is imposed along the material surfaces that have become separated by the displacement discontinuity, to ensure that the normal stress, σ_{33}, in the material abutting the surfaces is identical to that expected in the nonlinear material, for the given net displacement across the nonlinear zone (Fig. 2b). The single dominant crack is thus represented as two domains: one traction-free ($0 \le x_1 \le a_0$; $p = 0$) and one where line springs act ($a_0 \le x_1 \le a$; $p \ne 0$).[4] All the nonlinearity in the fracture problem is represented by the displacement discontinuity, $2u$, and the nonlinear constitutive behavior of the material in the damage zone is subsumed in the relationship $p(u)$.

Cohesive and bridged crack models

The leading edge of the nonlinear zone in the line-spring model, which lies at $x_1 = a$ in the plane symmetry conditions of Fig. 2, will be referred to in this paper as the crack tip, rather than the furthest progression of the traction-free domain ($x_1 = a_0$). The boundary condition imposed at the crack tip to close the fracture problem is taken to be that the stress–intensity factor at the crack tip is zero, so that the stress component, σ_{33}, in the material immediately ahead of the crack tip ($x_1 = a + \delta$) approaches the value $p(0)$ as $\delta \to 0$.

The critical step in applying the cohesive crack model is evaluating the relation, $p(u)$. Given this relation, all fracture properties can in principle be predicted. The relation will be inferred in this paper for one source of human cortical bone using data from the literature. The inferred relation will then be exploited to analyze the characteristics of the fracture process and to assess the validity of using LEFM to establish clinical correlations involving bone fracture.

[4] The name "line spring" derives from the fact that, in plane problems, the nonlinear tractions act along a single line. In problems of general symmetry, the discontinuity and tractions will be defined over an arbitrary surface, since the crack may advance on a nonstraight front or develop a curved fracture surface.

Results

Analysis of fracture data for human cortical bone

Data for human cadaveric cortical bone tested using compact–tension C(T) specimens have been presented previously by Nalla et al., together with observations of the mechanisms of crack resistance [35]. The tests and therefore all model formulations are cases of purely mode I fracture (negligible crack-sliding displacement), due to the symmetry of the specimen and the material. Plane-stress conditions will be assumed to apply and the crack will be assumed to advance along a straight front ($x_1 = a$, $x_3 = 0$).

A bilinear form will be assumed for $p(u)$, as illustrated in Fig. 3. This is consistent with deductions of the spatial distribution of tractions, $p(x_1)$, made in [35] using destructive specimen measurements. The parameters in the bilinear form will be evaluated by fitting test data for load vs. load-point displacement from refs. [35,36]. The degrees of freedom available in the bilinear form prove to be sufficient to fit these data to within the experimental noise.

Because a bilinear traction law has been assumed, it is convenient in discussing the results to refer to the fracture energy partition indicated in Fig. 3:

$$W_{total} = W_{tip} + W_{brid}, \tag{2a}$$

$$W_{tip} = 2\int_0^{u_0} p(u)\, du, \qquad W_{brid} = 2\int_{u_0}^{u_c} p(u)\, du. \tag{2b}$$

The subscripts "tip" and "brid" (for wake bridging) may suggest that a distinction exists between mechanisms acting near the

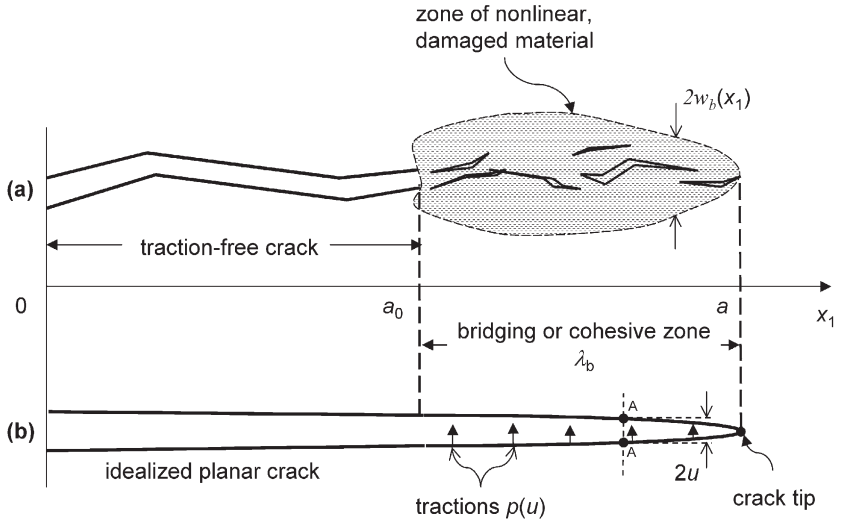

Fig. 2. Schematic of (a) discrete damage that has evolved into a single dominant crack with a diffuse crack tip damage zone and (b) the same system idealized as a planar crack with a bridging or cohesive zone. Tractions, p, are shown acting on one surface only, but must also act in equal magnitude and opposite sense on the other surface. As suggested, the tractions can vary in direction and magnitude along the cohesive zone. The displacement discontinuity across the crack is exemplified by the points marked A, which were coincident prior to fracture.

crack tip and in the further crack wake. However, the present analysis of fracture data cannot by itself resolve whether distinct mechanisms exist. The partition of Eqs. (2a) and (2b) is introduced purely for convenience and without any necessary physical significance.

For a monotonically decreasing cohesive traction law, the parameter p_c is equal to the unnotched tensile strength of the material under plane-stress conditions, in the idealization of the cohesive model (e.g., [5]). Higher stresses cannot be achieved because the material will suffer strain localization on some plane, followed by progression to failure at decreasing stresses. However, the measured tensile stress of unnotched bone specimens may differ from p_c, because strength is defect sensitive.

Compact–tension C(T) test data and analysis

Fig. 4 shows the C(T) test configuration used in ref. [35] and the location and orientation of the specimens in the bone. Three specimen tests will be analyzed here, among which the sample dimensions varied slightly (Table 1), leading to small but significant variations in the test data, especially the peak load. In the tests, a pre-crack was formed by machining a notch and then creating a small notch extension with tip radius of ~15 μm by polishing with a razor blade. The notch and pre-crack are similar to a natural crack with no wake bridging, so that their total length can be modeled as the initial value, c_0, of the traction-free crack length, a_0 (measured from the center-line of the loading hole). Values of c_0 varied as shown in Table 1. The specimen was oriented so that the crack propagated along the long axis (proximal–distal direction) of the bone.

Records of the load vs. load-point displacement (P vs. Δ) during the loading of the three specimens show an initial linear regime followed by nonlinearity (reduction of the tangent stiffness) until peak load is achieved, followed by a decline in the load (e.g., Fig. 5). The numerous downward spikes in the data mark instances of partial unloading used in [34] to measure the residual stiffness of the specimen. The test data beyond the peak load are inconsistent from specimen to specimen; in particular, the load in two cases falls anomalously fast. This suggests that excessive damage has been caused in the crack process zone by the repeated unloading events. In contrast, the unloading events had only a modest effect on the data before peak load and a single model can account for this domain very well for all specimens (see below).

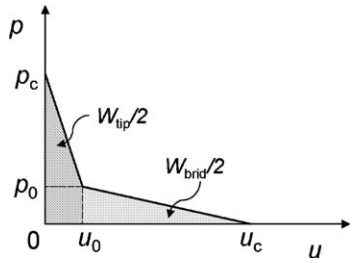

Fig. 3. A hypothetical cohesive traction law for a mode I cohesive zone.

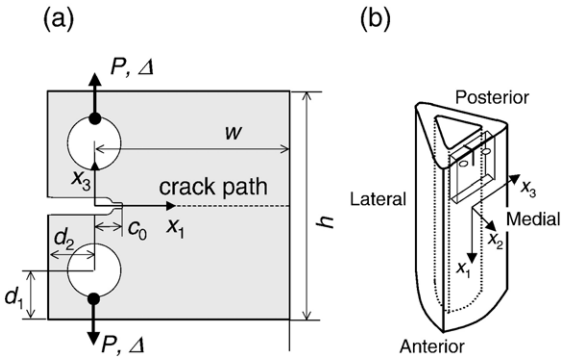

Fig. 4. (a) Geometry of the compact–tension specimens and (b) their location and orientation in the bone.

Table 1
Dimensions (mm) of experimental test specimens

	w	h	d_1	d_2	t	c_0
Specimen 1 [a]	15.7	17.0	4.0	3.8	2.5	3.6
Specimen 2 [b]	16.0	15.6	3.7	3.7	2.35	3.75
Specimen 3 [b]	17.0	16.8	4.1	3.8	1.9	4.1

[a] Taken from the right arm of the cadaver of a 37-year-old male.
[b] Taken from the left arm of the cadaver of a 41-year-old female.

The experiment was simulated by a finite-element calculation, using the commercial ABAQUS software (version 6.4; ABAQUS, Inc., Pawtucket, RI 02860). The possibility of a cohesive zone was introduced by incorporating a set of special cohesive elements, which allow a displacement discontinuity when a critical stress is reached at any point along the potential crack path. Within the cohesive elements, special numerical procedures are employed to allow the domain of displacement discontinuity to end part-way across an element, thus assuring smooth growth, and to assure that stress–traction continuity conditions are properly satisfied between the cohesive elements and the adjacent solid material elements at irregular features such as edges or corners. The numerical formulation of the cohesive elements is described in ref. [56]. The mode I cohesive traction law, $p(u)$, was assigned the piecewise linear form shown in Fig. 3. The loading pin was modeled as a rigid cylindrical shell coupled to the specimen by contact elements.

Elasticity of the specimen

Considerable variance exists in literature elasticity data for similar bone, with Young's moduli E_1 in the range 16–20 GPa and E_3 in the range 10–14 GPa [1,19,23,40,55]. The shear modulus μ_{31}, which is germane for the present C(T) tests, has not been measured for strain magnitudes relevant to these tests (it is a difficult orientation to test). Therefore, prior data being inadequate for quantitative analysis, we assume that the subject specimens are elastically orthotropic, which is a more reasonable idealization of cortical bone than isotropic elasticity, and use the test data themselves to evaluate the required elasticity coefficients.

Because no evidence of crack growth or damage could be seen in the experiments up to the point where the load–displacement data become nonlinear (Fig. 5), the slope, s_1, of the initial linear portion reflects only the elastic compliance of the specimen. For plane-stress conditions, s_1 is determined by the Young's moduli, E_1 and E_3, along the long axis and the circumferential direction of the bone, respectively, and by the shear modulus, μ_{31}.

The Young's moduli were assigned the values $E_1 = 16$ GPa and $E_3 = 12$ GPa. The shear modulus, μ_{31}, was then determined by fitting predictions in the elastic regime to the measured slope, s_1. For the test data of [34], $s_1 = 1050$ N/mm^2, which leads to $\mu_{31} = 1.5$ GPa.[5] Poisson's ratio in the x_1–x_3 plane, ν_{13}, was assigned the typical literature value, $\nu_{13} = 0.3$; ν_{31} follows from $\nu_{31}/E_3 = \nu_{13}/E_1$. The influence of the assumed values of the elastic constants on the deduced cohesive law was checked by varying E_1, E_3, and μ_{31} over ranges typical of the variance in literature values, always subject to the constraint of fitting the initial slope of the data. Predicted load–displacement curves using the modified elastic constants but the same optimal parameter values for the cohesive traction law were almost indistinguishable from those predicted with $E_1 = 16$ GPa and $E_3 = 12$ GPa.

Fitting the cohesive law

To evaluate the four coefficients, p_c, p_0, u_0, and u_c, of Fig. 3, a process of trial and error was used to minimize the residual difference between the prediction and the data of Fig. 5 (specimen 1 of Table 1). Because of the inconsistency in the data beyond peak load, the calibration fitting procedure used data only up to peak load in specimen 1. This fitting was always made to the envelope of the data, ignoring the unloading events.

Fitting revolves around several key features of the load–displacement data: (i) the slope of the linear region, reproduced by proper choice of elastic constants, (ii) the stress at the onset of the first significant nonlinearity, which is marked in Fig. 5, (iii) the predicted shape of the load–displacement curve between the onset of nonlinearity and peak load, and (iv) the location of the peak, in load and displacement.

Numerous trials showed that the onset of nonlinearity is sensitive to the contribution to the work of fracture that has been designated W_{tip} (Eqs. (2a) and (2b)), i.e., the traction law up to $u_3 = u_0$, but not to the parameters p_c p_0, and u_0, which define this part of the law, separately. Fitting the onset of nonlinearity yields $W_{tip} = 0.544$ kJ/m^2. The predicted onset of nonlinearity corresponds to the development in the model of a cohesive zone of small but nonzero length, along which p ranges from p_c

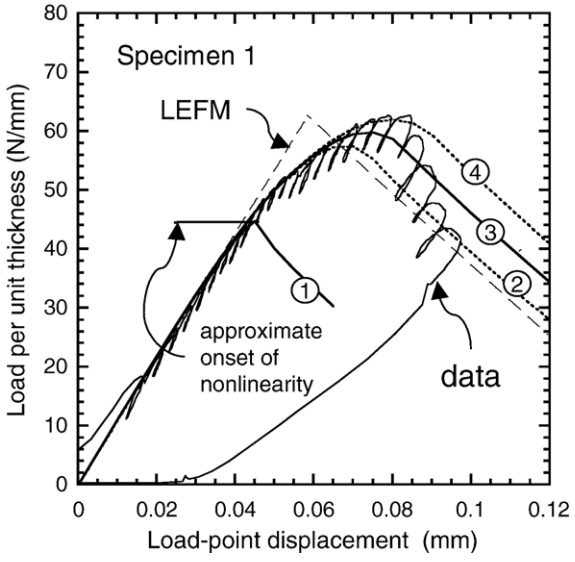

Fig. 5. Fitting fracture data (from [34]) in the form of normalized load vs. load-point displacement for one specimen (Specimen 1 of Table 1) of cortical humeral bone, taken from the humerus of a 37-year-old male.

[5] The displacement data reported in ref. [35] were the displacements of the actuator of the testing machine. As greater sensitivity is required for the present analysis, the same data are reported here, but with the displacements in the frame and load cell of the testing machine subtracted out. This gives a more accurate representation of the displacement of the material itself at the loading point of the specimen.

to approximately p_0. The influence of this small zone on the fracture process depends not on p_c alone, but on the integrated effect of the tractions in the zone, represented by W_{tip}. The first attainment of the condition $\sigma_{33} = p_c$ at the root of the notch extension ($x_1 = c_0$), and therefore the first activation of the cohesive zone, will have occurred considerably before this point in the load history. However, this earlier event has no significant immediate effect on the load–displacement curve; only when the crack opening at the root of the notch extension begins to exceed u_0 does the curve become noticeably nonlinear. Since the choice of p_c if W_{tip} is fixed also has no significant effect on the remainder of the load–displacement curve, p_c cannot be separately determined from the load–displacement data. A prescribed value is suggested for p_c, namely $p_c = 60 \pm 10$ MPa, consistent with literature data for the unnotched tensile strength in the circumferential direction of human Haversian bone [20,40].

The remaining parameters were varied to fit the data beyond the onset of nonlinearity. Three predictions that are optimal or near-optimal fits, with variance similar to the experimental uncertainty, are shown in Fig. 5 (trials 2–4). For trials 2–4, the traction law is the same in each case up to $u_3 = u_0$, preserving $W_{tip} = 0.544$ kJ/m^2. Also shown in Fig. 5 (trial 1) is the prediction found if the cohesive traction law is reduced to a simple triangle with work of fracture equal to $W_{total} = W_{tip} = 0.544$ kJ/m^2. The parameter values for the four trials are shown in Table 2.

At the onset of the nonlinear regime, the curve for trial 1 rises slightly and then falls, with the ultimate load barely exceeding the load to nonlinearity. The curves for trials 2–4 at first rise in unison in the nonlinear regime, before separating and reaching different ultimate loads. Beyond the ultimate load, they fall with similar slopes. The peak load and concomitant displacement rise with W_{brid} (or W_{total}).

Many other trials were run, including trials for traction laws in which the tail ($u > u_0$) was rectangular ($dp/du = 0$) or hardening ($dp/du > 0$). A qualitative summary of how features of the predicted load–displacement curves are sensitive to the different traction law parameters is as follows. The initial slope of the law, dp/du for small u, influences the slope of the predicted curve immediately following the onset of nonlinearity, but not for long. Most of the shape of the nonlinear regime is determined by the shape of the tail to the traction law (i.e., p for $u > u_0$) and the corresponding contribution to the work of fracture, W_{brid}. For hardening laws, the nonlinear regime is predicted to be concave, rather than convex, in contradiction of the experiments. For rectangular laws, the gradually softening behavior of the predicted curves up to the peak load is not reproduced; the predicted curve tends to be piece-wise linear, and the specimen displacement at ultimate tends to be underestimated, if the law is chosen to yield a correct prediction of the ultimate load.

Table 2
Parameter values of the cohesive traction law for the trials of Fig. 5

Trial	p_c(MPa)	p_0 (MPa)	u_0 (μm)	u_c (μm)	W_{tip} (kJ/m^2)	W_{brid} (kJ/m^2)
1	60	0	9.44	9.44	0.544	–
2	60	30	6.04	25.23	0.544	0.576
3	60	30	6.04	30.43	0.544	0.732
4	60	30	6.04	35.97	0.544	0.898

The deduced best-fit parameter values were taken to be those of Trial 4, since this trial fitted the data best up to peak load, including the value of the peak load, P_{max}, and the displacement at peak load, Δ_{max}. The best-fit values were $p_0 = 30 \pm 3$ MPa, $u_0 = 6 \pm 0.5$ μm, and $u_c = 36 \pm 4$ μm, with the errors estimated from uncertainty in the fitting of Trial 4 to the data. (Not that all of the errors can be independent, because of the constraint of satisfying the optimal value of W_{tip}.) These parameter values will be used in all further analyses. They imply $W_{brid} = 0.90 \pm 0.08$ kJ/m^2, which, together with the fitted value $W_{tip} = 0.54 \pm 0.05$ kJ/m^2, yields $W_{total} = 1.44 \pm 0.1$ kJ/m^2.

Test of predictive capability of cohesive law

Using the same elasticity and the same cohesive law (Trial 4) deduced by fitting the data of Fig. 5, predictions were attempted of the load–displacement data for specimens 2 and 3 of Table 1, which had different dimensions and different peak loads. The predictions fit the data well, being correct in the nonlinear behavior prior to peak load and the predicted values of P_{max} and Δ_{max} (Fig. 6). The goodness of fit can be partially quantified by the errors in P_{max} and Δ_{max} (Table 3). The error in P_{max} is only 1%, whereas its greatest variation from specimen to specimen is ~8%. The error in Δ_{max} is greater, but Δ_{max} is sensitive to small changes in the model or the calibrating data, being the location of an extremum. Prediction of the slope of the data following peak load is poor, with the data tending to fall much faster than the prediction, but this is expected, since accelerated damage due to the cycling sequence in the tests is not simulated by the model.

A direct comparison with the predictive capability of LEFM can be made as follows. The LEFM toughness, deduced from P_{max} according to standard ASTM procedures [2], gives a value of $K_{Ic} = 2.38$ MPa-m$^{-1/2}$ using the data of Fig. 5. The load–deflection curve predicted by LEFM has the simple shape marked "LEFM" in Fig. 5: a linear response (in the absence of global plasticity) up to peak load, followed by a monotonic decline in the load. The true shape of the load–displacement data and the value Δ_{max} cannot be reproduced, if K_{Ic} is chosen to fit P_{max}. Furthermore, the ability of LEFM to predict the response of the other two specimens is poor (Fig. 6 and Table 3). The error in P_{max} ranges up to 9% and that in Δ_{max} is 15–23%.

Discussion

Considerations of length scales

Within an order of magnitude, the length of the cohesive zone, $\lambda_b = a - a_0$ (Fig. 2), is given by a characteristic length, l_{ch}, which can be estimated from the cohesive law [5,16,26,42]. For a mode I crack:

$$l_{ch} = \frac{W_{total} E'}{p_c^2}, \tag{3}$$

where E' is the elastic constant of footnote 1, modified for orthotropic elasticity in [15,48], and taking the value $E' = 7.88$

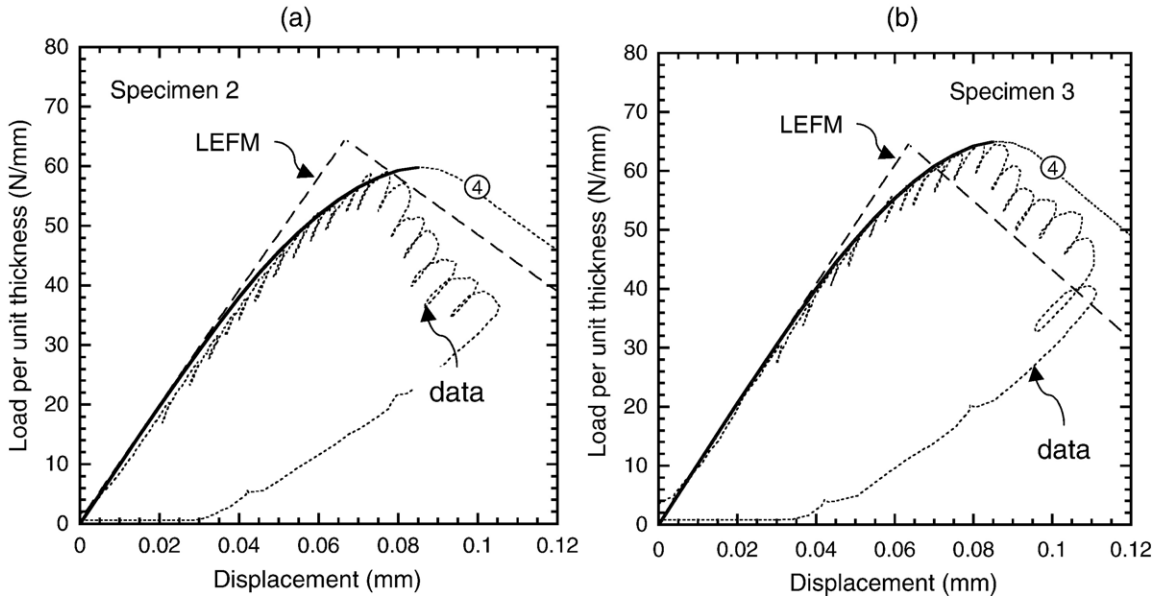

Fig. 6. Predictions of the load–displacement curves for two specimens (Specimens 2 and 3 of Table 1) of human cortical bone, taken from the humerus of a 41-year-old female (data from [34]).

GPa for the elastic constants E_1 = 16 GPa, E_3 = 12 GPa, and μ_{31} = 1.5 GPa (E' is not strongly sensitive to Poisson's ratios). With p_c = 60 MPa and W_{total} = 1.44 kJ/m^2, $l_{ch} \approx$ 3.2 mm, which is comparable to the zone length of 3.5 mm calculated in the simulations.

From these estimates, it is clear that only in the limit that the traction-free crack length, a_0, is much greater than l_{ch} and the damage zone does not approach other specimen boundaries, will the crack propagate under conditions that are well described by LEFM; indeed, only under these quite restrictive conditions will fracture toughness exist as a material constant, expressed, for example, as a critical value of the stress intensity, K_{Ic}, or strain-energy release rate, G_{Ic}. In this limit, referred to as small-scale bridging conditions, G_{Ic} will given by [10,46]:

$$G_{Ic} = W_{total} = 2\int_0^{u_c} p(u)du. \quad (4)$$

Implications for establishing clinical correlations involving bone quality

Proposed procedure for characterizing fracture properties

Since fracture is a primary mechanism of bone failure, especially in patients afflicted by age or osteoporosis, the cohesive law may be a preferred property on which to base clinical trials of the efficacy of drug and other therapies for ageing, osteoporosis, or other bone diseases. The question arises of what is the best experiment for determining the law.

The load vs. load-point curve taken alone contains sufficient information to determine the traction law with a degree of resolution of detail that is sufficient for predicting fracture behavior. These curves are readily available from standard fracture test procedures. The more difficult experiments of measuring crack profiles or mapping the spatial distribution of damage can certainly reveal additional information of clinical importance, but may not significantly improve the prediction of macroscopic features of fracture behavior. Such data would be relevant to models of local deformation events, rather than macroscopic cracking.

On the question of what test configuration should be preferred for acquiring load–displacement data for mode I fracture, the compact–tension test offers the following advantages. (1) Because it involves both bending and shear deformation, it provides, through the slope of the initial linear response, good information on the degree of elastic anisotropy of the material. Getting this information from the same specimen as that yielding fracture information has much merit, in view of the spatial inhomogeneity of bone. (2) Because of the presence of a compressive zone ahead of the growing crack, the process zone is relatively limited in extent, so that even in a specimen only 15–20 mm in total width, a

Table 3
Predictions of peak load and corresponding displacement using the cohesive model and LEFM

	Peak load per unit specimen thickness, P_{max} (N/mm)			Displacement at peak load, Δ_{max} (mm)		
	Data	Cohesive model prediction (% error)	LEFM prediction (% error)	Data	Cohesive model prediction (% error)	LEFM prediction (% error)
Specimen 1 (calibration specimen)	62.5	n/a	n/a	83	n/a	n/a
Specimen 2	59.1	59.8 (+1%)	64.5 (9%)	78	83 (+6%)	66 (−15%)
Specimen 3	64.2	65.0 (+1%)	64.4 (−0.3%)	83	85 (+2.5%)	64 (−23%)

steady-state zone is attained. Information about the complete traction law is therefore contained in the test.

Significance of the cohesive law in clinical studies

If one regards fracture as the primary failure mechanism of bone, then the reported weakness of correlation between bone quality and mineralization (e.g., [25]) is not surprising. The mineral phase in bone is certainly the stiffer and stronger phase, but fracture resistance in a composite such as bone is not determined by the properties of one phase alone. This is manifest at the fracture mechanics level from the present paper; if the mineral phase determined the fracture resistance of bone, then the fracture would be well described by LEFM, because the mineral phase, taken alone, is brittle. The fact that LEFM is inaccurate implies by itself, necessarily and very strongly, that the fracture process involves mechanisms beyond the mineral phase.

Such mechanisms have recently been sought in events occurring at the micrometer and even nanometer scales [4,24,36,44]. Principal putative energy absorbing mechanisms include plasticity in the collagen phase, crack deflection, especially along cement lines around osteons, diffuse microcracking, and the bridging of cracks by ductile phases (e.g., Fig. 1b). One might reasonably speculate, therefore, that bone quality is related not only or even primarily to mineralization, but also to the character of the collagen and other protein content of the bone and the morphological organization of the phases and structures in bone. The properties of the softer phases will, for example, have a strong influence on the efficacy of the crack bridging mechanism. The morphology of the composite, especially the connectivity of soft and hard phases, will govern crack deflection, the coalescence of microcracks, the elastic and nonlinear response of the bone prior to cracking, and other phenomena. Both the properties of the soft phases and the morphology of the bone might also, and perhaps more influentially for bone quality than mineralization, be changed by drug therapy.

The cohesive law, $p(u)$ (e.g., Fig. 3), contains a record of the effect of all internal mechanisms on the fracture performance of bone. All mechanisms at the micrometer and nanometer scales, crack deflection, microcracking, crack coalescence, plasticity, crack bridging, etc., act together to determine the relation $p(u)$. Furthermore, the internal mechanisms are relevant to macroscopic fracture (and perhaps therefore to mechanical aspects of bone quality) only as far as fracture test data determine $p(u)$, *and no further*. The extent to which the shape of the cohesive law can be determined from fracture data is limited exactly by the sensitivity of the experiment to changes in the material; the analysis here shows that mode I fracture data resolve no more than four independent scalar parameters in $p(u)$. (Analysis of engineering materials that have similar fracture characteristics [17,31] resolves a similar number of degrees of freedom.) If the fitting procedure cannot resolve further details in the traction law, then those further details of material behavior do not matter to the fracture observables. The determination of $p(u)$ from fracture data is an optimal measure of the role of internal mechanisms in bone fracture resistance.

We therefore advocate that fracture test data analyzed by nonlinear fracture modeling be used in establishing the efficacy of drug and other therapies that are purported to enhance bone quality. We propose the hypothesis that the parameters of the cohesive law will give a much more useful account of changes in bone quality than either mineralization or the single-parameter toughness of LEFM.

Concluding remarks

A cohesive fracture model has been formulated and applied to data for human femoral cortical bone. The central constitutive property in the model is the relation, $p(u)$, between the tractions supplied by nonlinear (failing) material across the fracture plane and the displacement discontinuity across the same plane. The relation $p(u)$ is hypothesized to be a material property for a given source of bone with given age and condition. The limited data analyzed here imply that a nonlinear model is superior to LEFM in accounting for the shape of load–displacement data and the peak load.

According to the nonlinear model, the onset of significant nonlinearity in the test data has been shown to be associated with the development of a cohesive zone of length ~ 0.5 mm over which tractions of 30–60 MPa exist, the upper value of stress being the conjectured critical value of the local stress for damage initiation. The cohesive zone length increases to approximately 3 mm as the crack propagates, concurring with experimental observations. Considerable variation of the cohesive zone length might be expected with the age and condition of the bone, shorter zones being associated with more brittle fracture, e.g., for aged or diseased bone.

Linear-elastic fracture mechanics can only be an internally consistent and accurate model of fracture in bone if the specimen and crack length both exceed the process-zone length. For the traction law deduced from fracture data for human cortical bone in the present work, this condition is unlikely to be met in any transverse fracture (normal to the long axis of the bone). Therefore, LEFM will not accurately describe the whole fracture process in human cortical bone.

The traction law, $p(u)$, offers an internally consistent approach to accounting for all macroscopic features of fracture. It includes, in the limit of long cracks (often longer than can be sustained in a bone), the fracture toughness, K_{Ic}, represented by LEFM; it also enables prediction of the initiation and propagation of fracture when the apparent toughness is not constant and can predict the effects of specimen shape and loading configuration. Because it describes the spatial distribution of stress over the nonlinear process zone associated with fracture, the traction law relates much more directly than does K_{Ic} to the underlying fracture processes.

Nomenclature

a	Crack length
a_0	Length of traction-free crack
b_{ij}	Voigt elastic constants
c_0	Length of initial notch plus notch extension
d_1, d_2	Specimen dimensions
δ	Small quantity

Δ	Load-point displacement
E, E_I	Young's moduli
E'	Combination of elastic constants
ε_{ij}	Component of strain
$\varepsilon_{ij}^{(c)}$	Critical value of strain
$\varepsilon_{ij}^{(p)}$	Component of plastic strain
f	Fitting function
G_i	Strain energy release rates, i = I, II, III
G_{ic}	Critical value of G_i, i = I, II, III
h	Specimen height
K_I	Stress–intensity factor in mode I (tensile opening)
K_{Ic}	Critical value of K_I at fracture
K_b	Reduction of stress–intensity factor due to bridging
$K_R(a)$	Apparent critical stress–intensity factor at crack length a
λ_b	Length of bridging or process zone
l_{ch}	Characteristic length of traction–displacement law
LEFM	Linear-elastic fracture mechanics
μ, μ_{ij}	Engineering shear moduli
N	Elapsed load cycles
ν, ν_{ij}	Poisson's ratios
w_b	Half-width of bridging or process zone
w_m	Maximum value of ω_b
P	Load per unit specimen thickness
p	Mode I traction
p_c, p_0	Parameters of traction–displacement law
s_1	Initial slope of load vs. load-point displacement data
σ_{ij}	Component of stress
t	Specimen thickness
τ	Time
u	Crack opening displacement
u_c, u_0	Parameters of traction–displacement law
x	Spatial (x_1, x_2, x_3) coordinates
w	Specimen width
W_i	Total and partial values of the work of fracture, i = total, dip, brid
Y	a constant

Acknowledgments

QDY received partial support from a Rockwell Scientific seedling project. RKN was supported by the National Institutes of Health under Grant No. 5R01 DE015633 and ROR by the Director, Office of Science, Office of Basic Energy Science, Division of Materials Sciences and Engineering, Department of Energy under No. DE-AC03-76SF00098.

References

[1] Ashman RB, Cowin SC, Van Buskirk WC, Rice JC. A continuous wave technique for the measurement of the elastic properties of cortical bone. J Biomech 1984;17:349–61.
[2] ASTM E 399-90. Annual book of ASTM standards. West Conshohocken, Pennsylvania: American Society of Testing and Materials; 2001 [Reapproved 1997].
[3] Aveston J, Cooper GA, Kelly A. Single and multiple fracture. The properties of fiber composites. National Physical Laboratory, London: IPC Science and Technology Press Ltd., Guildford, Surrey; 1971 p. 15–24.
[4] Ballarini R, Kayacan R, Ulm FJ, Belytschko T, Heuer AH. Biological structures mitigate catastrophic fracture through various strategies; Int J Fract 2005; 135:189–99.
[5] Bao G, Suo Z. Remarks on crack-bridging concepts. Appl Mech Rev 1992;24:355–66.
[6] Barenblatt GI. The mathematical theory of equilibrium cracks in brittle fracture. In: Dryden HL, Von Karman T, editors. Advances in applied mechanics, vol. 2. Academic Press; 1962. p. 55–129.
[7] Behiri JC, Bonfield W. Fracture mechanics of bone—The effects of density, specimen thickness and crack velocity on longitudinal fracture. J Biomech 1984;17:25–34.
[8] Behiri JC, Bonfield W. Orientation dependence of the fracture mechanics of cortical bone. J Biomech 1989;22:863–72.
[9] Brown CU, Yeni YN, Norman TL. Fracture toughness is dependent on bone location—A study of the femoral neck, femoral shaft, and the tibial shaft. J Biomed Mater Res 2000;49:380–9.
[10] Budiansky B, Hutchinson JW, Evans AG. Matrix fracture in fiber reinforced ceramics. J Mech Phys Solids 1986;34:167–89.
[11] Carpinteri A, Massabò R. Bridged versus cohesive crack in the flexural behavior of brittle matrix composites. Int J Fract 1996;81:125–45.
[12] Cottrell AH. Mechanics of fracture. Tewksbury symposium on fracture. Melbourne, Australia: University of Melbourne; 1963. p. 1–27.
[13] Cox BN. Extrinsic factors in the mechanics of bridged cracks. Acta Metall Mater 1991;39:1189–201.
[14] Cox BN, Lo CS. Load ratio, notch, and scale effects for bridged cracks in fibrous composites. Acta Metall Mater 1992;40:69–80.
[15] Cox BN, Lo CS. Simple approximations for bridged cracks in fibrous composites. Acta Metall Mater 1992;40:1487–96.
[16] Cox BN, Marshall DB. Concepts for bridged cracks in fracture and fatigue. Acta Metall Mater 1994;42:341–63.
[17] Cox BN, Marshall DB. The determination of crack bridging forces. Int J Fract 1991;49:159–76.
[18] Cox BN, Marshall DB. Stable and unstable solutions for bridged cracks in various specimens. Acta Metall Mater 1991;39:579–89.
[19] Currey JD. Mechanical properties of vertebrate hard tissues. Proc Inst Mech Eng 1998;212H:399–412.
[20] Currey JD. 'Osteons' in biomechanical literature. J Biomech 1982;15:717.
[21] Dugdale DS. Yielding in steel sheets containing slits. J Mech Phys Solids 1960;8:100–4.
[22] Fantner GE, Birkedal H, Kindt JH, Hassenkam T, Weaver JC, Cutroni JA, et al. Influence of the degradation of the organic matrix on the microscopic fracture behavior of trabecular bone. Bone 2004;35:1013–22.
[23] Fung YC. Biomechanics: mechanical properties of living tissues. New York: Springer-Verlag; 1993.
[24] Gao HJ, Ji BH, Jager IL, Arzt E, Fratzl P. Materials become insensitive to flaws at nanoscale: Lessons from nature. Proc Natl Acad Sci U S A 2003;100:5597–600.
[25] Heaney RP. Is the paradigm shifting? Bone 2003;33:457–65.
[26] Hillerborg A, Modeer M, Petersson PE. Analysis of crack formation and crack growth in concrete by means of fracture mechanics and finite elements. Cem Concr Res 1976;6:773–82.
[27] Kahler B, Swain MV, Moule A. Fracture-toughening mechanisms responsible for differences in work to fracture of hydrated and dehydrated dentine. Biomechanics 2003;36:229–37.
[28] Kruzic JJ, Nalla RK, Kinney JH, Ritchie RO. Mechanistic aspects of in vitro fatigue-crack growth in dentin. Biomaterials 2005;26: 1195–1204.
[29] Li VC, Wang Y, Backer S. A micromechanical model of tension-softening and bridging toughening of short random fiber reinforced brittle matrix composites. J Mech Phys Solids 1991;39:607–25.
[30] Malik CL, Stover SM, Martin RB, Gibeling JC. Equine cortical bone exhibits rising R-curve fracture mechanics. J Biomech 2003;36:191–8.
[31] Massabò R, Mumm DR, Cox BN. Characterizing mode II delamination cracks in stitched composites. Int J Fract 1998;92:1–38.
[32] Nalla RK, Kinney JH, Ritchie RO. Mechanistic fracture criteria for the failure of human cortical bone. Nat Mater 2003;2:164–8.

[33] Nalla RK, Kruzic JJ, Kinney JH, Ritchie RO. Aspects of fatigue-crack growth in human cortical bone: importance of both cycles- and time- to failure. Biomaterials 2005;26:2181–93.
[34] Nalla RK, Kruzic JJ, Kinney JH, Ritchie RO. Effect of aging on the toughness of human cortical bone: evaluation by *R*-curves. Bone 2004;35:1240–6.
[35] Nalla RK, Kruzic JJ, Kinney JH, Ritchie RO. Mechanistic aspects of fracture and *R*-curve behavior in human cortical bone. Biomaterials 2005;26:217–31.
[36] Nalla RK, Kruzic JJ, Ritchie RO. On the origin of the toughness of mineralized tissue: microcracking or crack bridging? Bone 2004;34: 790–8.
[37] Nalla RK, Stölken JS, Kinney JH, Ritchie RO. Fracture in human cortical bone: local fracture criteria and toughening mechanisms. J Biomech 2005;38:1517–25.
[38] Norman TL, Vashishth D, Burr DB. Fracture toughness of human bone under tension. J Biomech 1995;28:309–20.
[39] Phelps JB, Hubbard GB, Wang X, Agrawal CM. Microstructural heterogeneity and the fracture toughness of bone. J Biomed Mater Res 2000;51:471–735.
[40] Reilly DT, Burstein AH. The elastic and ultimate properties of compact bone tissue. J Biomech 1975;8:393–405.
[41] Rho J-Y, Kuhn-Spearing L, Zioupos P. Mechanical properties and the hierarchical structure of bone. Med Eng Phys 1998;20:92–102.
[42] Rice JR. The mechanics of earthquake rupture. In: Dziewonski AM, Boschi E, editors. International school of physics "E. Fermi", course 78. Italian Physical Society/North Holland Publ. Co; 1980.
[43] Ritchie RO. Mechanisms of fatigue crack propagation in metals, ceramics and composites: role of crack-tip shielding. Mater Sci Eng 1988;103:15–28.
[44] Ritchie RO, Kinney JH, Kruzic JJ, Nalla RK. A fracture mechanics and mechanistic approach to the failure of cortical bone. Fatigue Fract Eng Mater Struct 2005;28:1–27.
[45] Rose LRF. Crack reinforcement by distributed springs. J Mech Phys Solids 1987;34:383–405.
[46] Rose LRF. A cracked plate repaired by bonded reinforcement. Int J Fract 1982;18:135–44.
[47] Saxena A. Nonlinear fracture mechanics for engineers. Boca Raton, FL: CRC Press; 1998.
[48] Sih GC, Paris PC, Irwin GR. On cracks in rectilinearly anisotropic bodies. Int J Fract Mech 1965;1:189–203.
[49] Sneddon IN, Lowengrub M. Crack problems in the classical theory of elasticity. New York: Wiley; 1969.
[50] Suo Z, Bao G, Fan B. Delamination *R*-curve phenomena due to damage. J Mech Phys Solids 1992;40:1–16.
[51] Vashishth D. Rising crack–growth–resistance behavior in cortical bone: implications for toughness measurements. J Biomech 2004;37:943–6.
[52] Vashishth D, Behiri JC, Bonfield W. Crack growth resistance in cortical bone: concept of microcrack toughening. J Biomech 1997;30:763–9.
[53] Vashishth D, Tanner KE, Bonfield W. Experimental validation of a microcracking-based toughening mechanism for cortical bone. J Biomech 2003;36:121–4.
[54] Wright TM, Hayes WC. Fracture mechanics parameters for compact bone-effects of density and specimen thickness. J Biomech 1977;10:419–30.
[55] Yamada H. Strength of biological materials. Baltimore: Williams and Wilkins; 1970.
[56] Yang QD, Cox BN. Cohesive models for damage evolution in laminated composites. Int J Fract 2005;133:107–37.
[57] Yeni YN, Brown CU, Norman TL. Influence of bone composition and apparent density on fracture toughness of the human femur and tibia. Bone 1998;22:79–84.
[58] Yeni YN, Brown CU, Wang Z, Norman TL. The influence of bone morphology on fracture toughness of the human femur and tibia. Bone 1997;21:453–9.
[59] Yeni YN, Fyhrie DP. A rate-dependent microcrack-bridging model that can explain the strain rate dependency of cortical bone apparent yield strength. J Biomech 2003;36:1343–53.